In Vivo Characterization of Cortical Noradrenergic Activity During Motor Learning Using an Optical Noradrenaline Sensor in Mice

Nathaniel Jones

A thesis submitted in partial fulfillment of the requirements for the
Master's degree in Neuroscience

Department of Cellular and Molecular Medicine
Faculty of Medicine
University of Ottawa

Abstract

The locus coeruleus (LC) projects ubiquitously to the cortex, and noradrenaline (NA) exerts powerful neuromodulatory control on cortical excitation and inhibition. Previous work has shown that NA plays an important role in motor processes, and further posits that dysregulation in NA function could be one of the culprits of motor-related deficits in many neurodevelopmental disorders, including Autism Spectrum Disorder. In order to characterize the change in NA levels during motor learning in awake and behaving mice, I employed a newly developed optical NA sensor, combined with *in vivo* two-photon imaging, to visualize spatiotemporal activation patterns of NA in the motor cortex. This experimental approach allows us to track and chronically image the same region of the motor cortex over multiple days, thus permitting the characterization of NA activity throughout the entirety of the motor learning process. I found that NA levels increase significantly during the initial phase of learning, which coincides with the structural and functional plastic changes that have been previously reported in the motor cortex during early stages of motor learning. The NA activity returns to baseline levels as the mice develop their movement strategy; however, the regions of NA release become more spatially clustered during the learning process. The results reported in this thesis provide a novel glimpse into the dynamics of NA activity in the motor cortex during motor learning, and it will provide new direction for the development of therapeutic strategies and diagnostic criteria for motor-related dysfunction in neurodevelopmental diseases.

Table of Contents

Acknowledgements

First and foremost, I would like to thank my family for their incredible and unwavering support throughout my project, and for the perseverance they have instilled in me. My mother, for hearkening my every concern and complaint; my father, for evening Fifa matches to relieve stress; my brothers, for contributing to the maintenance of my sanity with music, memes, and news of home; my friends, for being a constant reminder of who I am and what I value.

I would also like to thank my labmates and colleagues for furthering my education, broadening my understanding, and my approach to research. I would like to thank Dr Xuming Yin, PhD, and his wife Liwen, M.A., for training and assisting me in many of the techniques used in the project. Similarly, I would like to thank my labmates, PhD candidates Nima Raman and Candice Lee, for invaluable discussions regarding my project, and Pablo Serrano, BSc, for facilitating my remote access to the lab. I would further like to extend my thanks to each member of the Chen Lab for important feedback on my project throughout the process. For proofreading this thesis, I would like to sincerely thank my labmate Candice Lee and my long-time colleague J. Ellen.

Finally, I would like to thank my thesis supervisor, Dr Simon Chen, PhD, for the guidance, wisdom, feedback, and support that facilitated the completion of my project. Simon has been instrumental in the conception and experimental design of this project, and fundamental in its realization.

To those mentioned, I owe an infinite debt of gratitude; without them my project would not have been possible. Cheers.

Introduction

Autism Spectrum Disorder

Autism spectrum disorder (ASD) is a neurodevelopmental disorder characterized in the Diagnostic and Statistical Manual of Mental Disorders (DSM-V) by language, cognitive, or social impairments, often combined with repetitive behavior or movements. ASD impacts an increasing number of Canadians every year, with the incidence rate rising from approximately 5 in 10,000 just 20 years ago, up to 20 in 10,000 in 2015 (NASS 2018). Estimates from the CDC indicate that over 1 million children in North America are afflicted—likely a low range estimate considering undiagnosed children. Family members may also be impacted by these diagnoses, for example, in 2005, US medical costs for children with ASD were 6 times higher than for typically developing children. Cognitive and social deficits are commonly associated with ASD and thus affect the primary modes of assessment. The DSM-V criteria for ASD thoroughly outline social and behavioral symptoms, with severity determined by communicative impairments and repetitive behavior. Currently, diagnoses can be reliably made after approximately 2 years of age[1] and indeed, the majority (80%) of diagnoses are made before the age of 10, and over 50% by age 6, which underscores the early emergence of ASD.

Motor-Related Symptoms & Diagnostic Criteria

Most ASD diagnoses are made during childhood, as afflicted individuals often undershoot social and cognitive developmental milestones. Recent studies indicate, however, that ASD is associated with impaired performance and delayed learning in motor tasks[2]. Voluntary movements originate from primary motor cortex (M1) activity, suggesting that motor

development may be additionally impacted by ASDs, further compounding social and cognitive developmental delays. In fact, these motor symptoms typically present earlier than social or cognitive indicators, with symptoms of motor abnormalities present as early as 6 months of age[3]. Furthermore, parent reports of movement difficulties and motor issues in young infants and toddlers can provide symptomatic insight prior to an age when stable diagnoses can be made, and further predict language and motor development[1,7]. Despite this, diagnoses hinge mainly on social and cognitive symptoms, which cannot be readily assessed in infants and toddlers.

Once a diagnosis of ASD is made, many context dependant approaches can be employed to intervene and ameliorate symptoms or improve outcomes. Intervention can take many forms including behavioral, family-based, and therapy-based, or otherwise a combination thereof. For example, intervention implemented by both parent and clinician has been shown to improve spoken language outcomes in children with ASD[4]. As early as 2010, it was established by work such as the Early Start Denver Model, that a comprehensive developmental and behavioral intervention for toddlers can be efficacious in reducing the severity of diagnosis[5]. Motor control can be a predictor for speech fluency outcomes in ASD children[6,7], and speech development delays have been important diagnostic criteria for ASD since the DSM-IV update in 2000. Evidence of difficulties with motor control often predates and underlies diagnostic symptoms, therefore, elucidating the process of motor learning will be crucial to expanding the clinical and basic understanding of ASD, and may facilitate earlier intervention and diagnosis for improved treatment and patient outcome.

Delayed Motor Learning in 16p.11.2 deletion mice

ASDs are genetically heritable and caused by various genetic mutations. Microdeletions cause the deletion of genes or groups of genes from particular loci of chromosomes; the removal of these genes are often cited as factors in ASD[31,32]. One of the most common microdeletions is that of the 16p11.2 gene locus, affecting approximately 1% of ASD diagnosed individuals, and resulting in the deletion of almost 30 genes. Genetic manipulation has provided an experimental mouse line heterozygous for the deletion of a syntenic region in murine DNA (7qF4), and vitally, displaying behavior reminiscent of human ASD phenotypes such as stereotyped behavior and motor movements[8]. With this powerful genetically engineered tool, we can gather insight on the impact of ASD on motor function in a behavioral capacity. To wit, our lab has recently uncovered delayed motor learning in 16p11.2 deletion mice, which is apparent in both rotarod task and in our newly developed head-fixed spinning-disk task. This learning delay is distinct from an overall motor impairment in that mutant mice are capable of learning the task, but do so at a reduced rate. Moreover, cFos staining revealed 16p11.2 deletion mice have a lesser degree of LC activation after 1 session of training as compared to WT mice (Figure 1a). Noradrenergic axonal staining in M1 also revealed a significant reduction of M1 L2/3 innervation by LC-NA axons in 16p11.2 deletion mice that was region- and layer-specific (Figure 1b), suggesting reduced NA release in mutant mice.

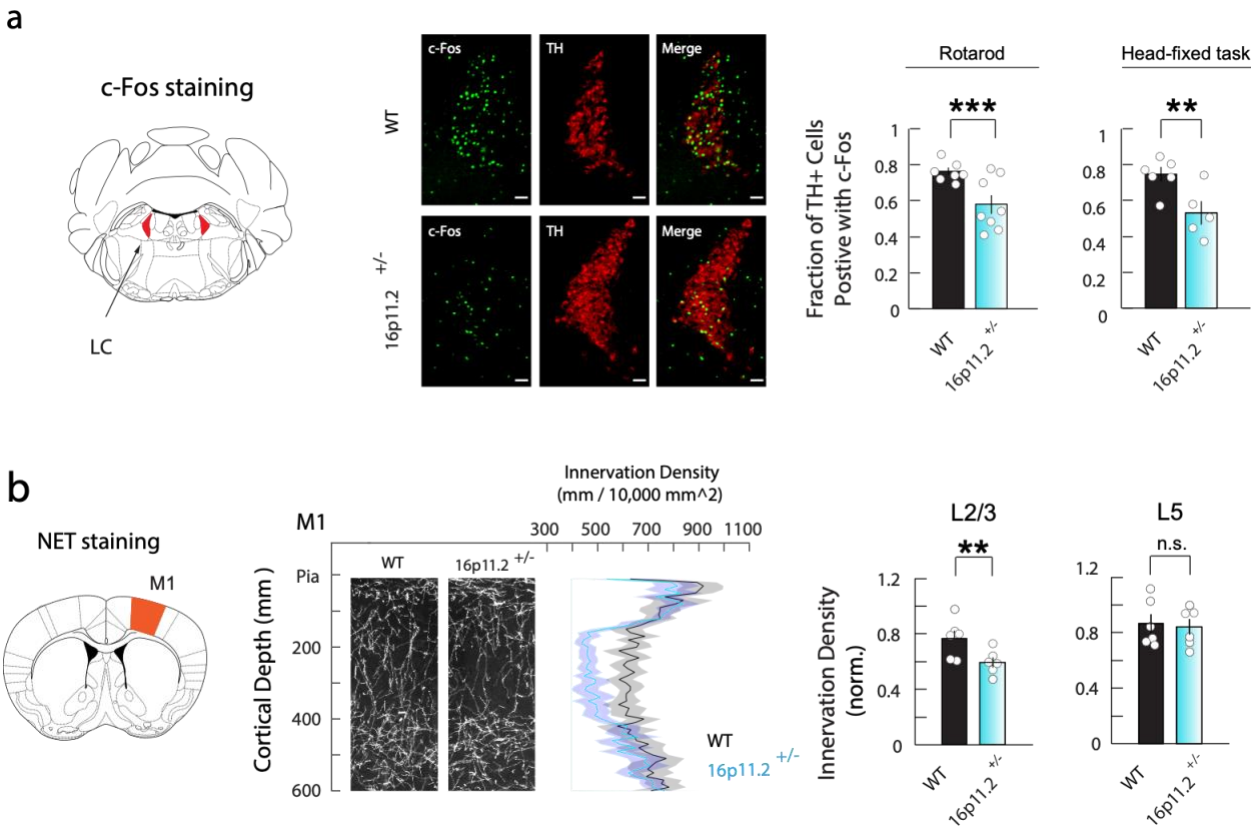

Figure 1: **Delayed motor learning a)** left: schematic of c-Fos staining, LC delineated in orange, center: center-left column shows cFos staining of LC, center-middle shows TH+ cells, center-right shows merged images-top and bottom indicate WT and 16p11.2 deletion mice respectively, right: mean percentage quantification of TH+ overlap with cFos+ after a single rotarod training session (n=7-8 mice), or single rotating-disk training (n=5-6 mice), respectively, in WT and mutant mice. One-tailed bootstrap test. Scale bar = 50 µm. **b)** left: schematic of M1 staining, M1 delineated in orange, center: cortical innervation density comparison between WT (center-left, black) and 16p11.2 deletion mice (center-right, turquoise), right: quantification of M1 innervation density by layer and mouse genotype.

We further addressed the putative reduced NA activity by employing a Designer Receptors Exclusively Activated by Designer Drugs (DREADDs) approach, where activation of excitatory designer receptors expressed in LC-NA neurons partially rescued behavioral results in both rotarod and spinning-disk tasks[9]. Our results indicate the involvement of LC-NA in motor action and highlight NA as a culprit in delayed motor learning, particularly its activity in the motor cortex.

Motor Cortex

The role of the primary motor cortex in voluntary movement is well established, however, the mechanisms thereof are not yet fully understood. M1 is thought to be responsible for the formation and maintenance of motor memory representations[10, 11]. To generate these motor representations, M1 coordinates activity between upper cortical layers that receive thalamic input and lower layers that project cortical output to thalamus, and similarly coordinates between neighboring motor and sensory regions to optimize information flow during motor behavior[12,13]. Thus, disruption of M1 circuitry can influence the acquisition of fine motor skills—for example, those involved in speech articulation—thereby exacerbating social and cognitive deficits. Cortical information flow is essential to proper motor function, and current prevalent views of ASD implicate an imbalance of excitation and inhibition in the neocortex[14], a crucial and delicate feature of pre-natal and early post-natal cortical development[15].

Studies investigating motor or movement corrections—such as induced error in a reaching task via stimulation of the motor cortex[16], or the mechanical perturbation of outstretched limbs[17] —underline the importance of maintaining and modulating cortical circuitry appropriately for motor behavior. Therefore, a characterization of M1 functional and network changes throughout motor learning, should be considered along with the role of NA activity in the motor learning process.

Motor Learning

Importantly, motor learning is associated with neuronal plasticity in the motor cortex. The role of M1 in voluntary motor action is highly phylogenetically conserved, highlighting the

importance of flexible motor control. Requirements of such flexibility place a substantial workload on motor memory, which is reliant on the formation of neuronal ensembles, or groups of neurons displaying a reproducible spatiotemporal activation pattern during a learned motor movement[21]. Thus, the execution of skilled and reproducible motor movements requires a high degree of repetition, which contributes to the relatively long acquisition period as compared to other forms of learning[18]. In early stages of motor learning, there is a high degree of variability in the execution and strategy of novel motor behavior; this variability often tapers off in later stages of learning when subjects develop more expertise[19].

The mechanistic underpinnings of this learning process are still unclear, although numerous hypotheses exist. Previous studies have shown that motor learning is accompanied by changes in spine dynamics and synaptic plasticity, increased ensemble activity with emergent spatiotemporal reproducibility[20,21,22], and layer-specific network refinement resulting in differential activation patterns in the motor cortex[13].

Noradrenaline in Learning

Recent evidence has underlined the involvement of neuromodulators in locomotion and overall arousal/behavioral state[23]. More specifically, NA has been found to modulate synaptic plasticity by regulating dendritic excitability in L5 pyramidal neurons[24,25], and was shown to be necessary for motor execution[26]. LC-NA has been shown to induce cortical plasticity in auditory cortex, and to improve learning speed when coupled with coupled with an auditory stimulus[27]. NA activity originating from LC, but projecting to separate ensembles, has also been shown to exert control over opposing learning states[28], which points to the possibility of some gating mechanism via NA. In addition, electrophysiological studies[29], and rabies tracing[30] have shown

the high level of heterogeneous connectivity between LC and motor-related areas, contrasting with the classical view of LC as a homogeneous NA factory projecting indiscriminately to the forebrain. Taken together with our delayed motor learning results, these lines of evidence converge to suggest a crucial modulatory role of NA in motor learning and acquisition.

Research Statement

Two-photon imaging studies have generally employed fluorescent calcium indicators and used calcium transients as a measure of pyramidal cell activity, but due to a plethora of technical limitations, have thus far marginalised the role of neuromodulatory action in these motor circuits. Here, using the newly developed NE1m, I have uncovered a role for NA in wild type (WT) mice in the motor cortex throughout motor learning, providing crucial insight into the neuromodulatory mechanisms thereof. Investigating the role for NA can function as a stepping stone towards understanding ASD-related circuit dysfunction, such as has been demonstrated in 16p11.2 deletion mice, *Fmr1*$^{-/-}$ mice[31], and *Shank3* mice[32]. Because neuromodulators like NA exert such a strong influence on plasticity, understanding neuromodulatory action during motor learning will be paramount to improving diagnostic tests to provide critical early intervention and treatment for ASDs.

Aims & Hypothesis

Aims

1. To characterize the NA sensor NE1m for *in vivo* two-photon imaging.

2. To investigate the role of NA in motor learning in a novel head-fixed behavioral task.

Hypothesis

1. I hypothesize that M1 NA levels in WT mice will increase in the early training sessions of a head-fixed motor learning task but will exhibit an overall decrease over the course of the motor learning.

Results

Behavior

Motor Learning Coincides with Reduction in Variability of Movement Dynamics

In our novel, non-reward-associated head-fixed motor learning task, mice were trained (1 hour/session, 1 session/day, 12 sessions) to run on a bi-directional rotating disk (Figure 2a). Running epochs (RE) were defined as an instance of surpassing a velocity threshold for 3 or more seconds (see Methods). Performance in the task was measured with various behavior-based learning metrics. For example, an increased distance travelled per session on the disk, longer duration of REs, and higher RE count with learning (Figure 2b,c,d). These metrics were chosen to measure performance as their trajectory across sessions delineates running capability and execution. Notably, this head-fixed task requires the animals to learn an alternative running posture, necessitating voluntary and intentional movements which invoke the motor cortex (Figure 2e).

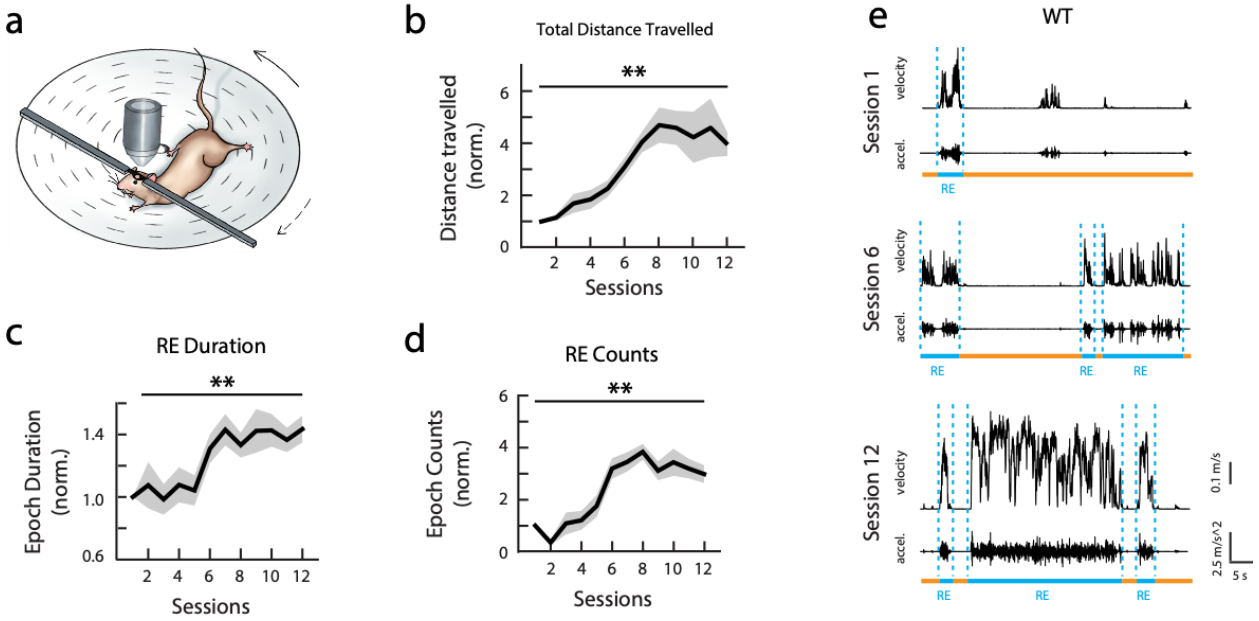

Figure 2: Running behavior metrics a) schematic of spinning-disk task. **b)** Improved running performance across 12 training sessions normalized to the first session. Note a significant increase in the total distance travelled over 12 sessions of training ($p < 0.001$; 1-way ANOVA; n = 7-10 mice; solid line, mean normalized distance travelled of each group; shading, s.e.m.). **c-d).** Normalized RE counts (**c**) and duration (**d**) across all 12 training sessions. **e**) Representative REs and their corresponding velocity and acceleration from the early (top, session 1), intermediate (middle, session 6), and expert (bottom, session 12) training levels from WT mice ($p > 0.05$, 2-way ANOVA; n = 7-10 mice; solid line, mean counts of each group; shading, s.e.m.). * $p < 0.05$, *** $p < 0.001$. Error bars indicate s.e.m.

First, to rigorously quantify the performance of mice in this motor learning task, I employed DeepLabCut, a machine learning algorithm used to track and consistently label relevant physical features in an unbiased fashion. To assess postural changes over the course of learning, I used DeepLabCut to track coordinates of the head, nape, thorax, and sacrum throughout each behavioral session (Figure 3a). As a reduction in movement variability has been shown to be associated with motor learning[18], I developed an approach to measure the variance of movement dynamics in our spinning-disk task. The head-fixed nature of the task limits the range of motion for the mouse, producing a fan-shaped distribution of label coordinates (Figure 3b). I therefore isolated coordinates labeled during REs (Figure 3c), and calculated the angle generated at the vertex of the nape by vectors intersecting two opposing, extreme sacrum points (see Methods). From this index of displacement, I calculated the relative variance (V_r) of the angles generated in each session, as well as their coefficient of variation (*CV*), and found that both V_r and *CV* are reduced with training (Figure 3e,f). Our results are in line with previous studies showing reduced variance as a result of learning a motor task; further buttressed by other performance metrics in the head-fixed spinning-disk task described above.

Figure 3: Behavioral variability decreases with experience a) top: schematic of spinning-disk task under infrared imaging camera. Colored points represent the head (maroon), nape (blue), thorax (turquoise), and sacrum (yellow). bottom: behavioral imaging paradigm. Mice undergo craniotomy/injection surgery 42 days postnatal. After 2-3 weeks of recovery, mice are habituated to the spinning-disk under the infrared camera for 3-5 days, with 5-10 minutes of habituation each day. Mice are then imaged each day of behavioral training. **b**) exemplar plot of labeled point distribution across one entire early training session. **c)** coordinates from two isolated running epochs from one mouse across four sessions: first column, session 1; second column, session 4; third column, session 8; fourth column, session 12. AU, arbitrary units. **d)** Mean relative variance of the RE generated angles is steadily reduced with motor learning ($p < 0.01$; 1-way ANOVA; Solid line, mean variance; shading, s.e.m.). **e)** The coefficient of variance of the RE generated angles also steadily decreases with motor learning ($p < 0.05$; 1-way ANOVA; Solid line, coefficient of variance; shading, s.e.m.).

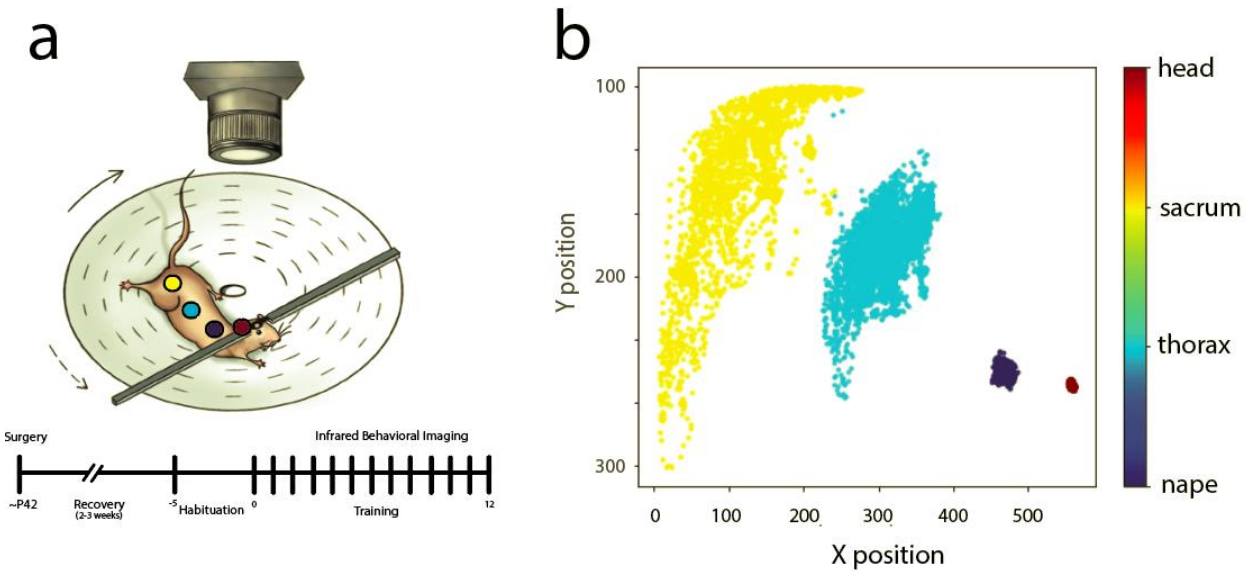
a
Surgery
Infrared Behavioral Imaging
~P42
Recovery
(2-3 weeks)
-5
Habituation
0
Training
12
b
head
sacrum
thorax
nape
Y position
X position
100
200
300
0
100
200
300
400
500

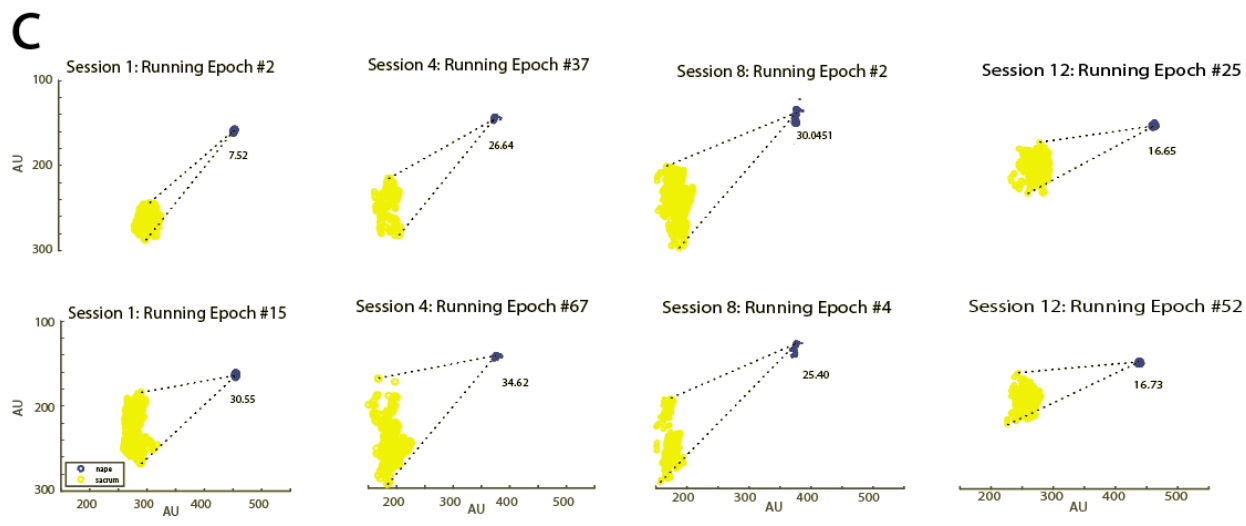
c
Session 1: Running Epoch #2
Session 4: Running Epoch #37
Session 8: Running Epoch #2
Session 12: Running Epoch #25
Session 1: Running Epoch #15
Session 4: Running Epoch #67
Session 8: Running Epoch #4
Session 12: Running Epoch #52
AU
7.52
26.64
30.0451
16.65
30.55
34.62
25.40
16.73
nape
sacrum

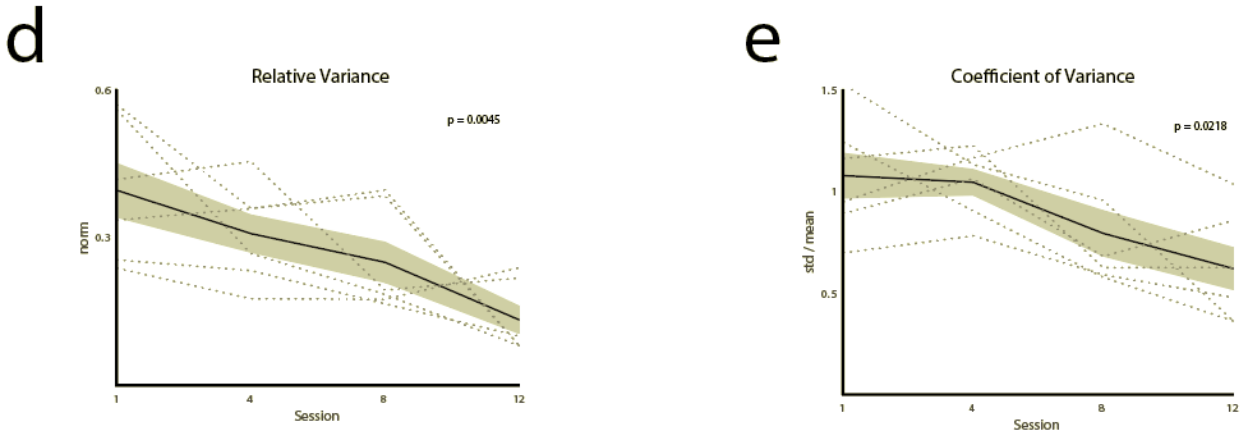
d
Relative Variance
p = 0.0045
norm
Session
e
Coefficient of Variance
p = 0.0218
std / mean
Session

Sensor Characterization

NE1m is Abundantly Expressed in M1 Neurites

Next, I set out to investigate NA activity over the course of motor learning by employing two-photon imaging of a newly developed NA sensor, NE1m. Several lines of evidence, along with recent work from our lab, point to a crucial role for NA in the motor cortex. The recent development of an optical sensor to observe NA activity is exciting for many reasons, as it provides an unprecedented non-invasive method of visualizing neuromodulatory activity in awake and behaving mice. NE1m is derived from human α2-adrenergic receptor (α2-AR), which exhibits more robust membrane trafficking compared to other ARs (α1-, α2b-, and β-ARs). The third intracellular loop (ICL_3) undergoes a conformation change upon NA-induced activation of α2-AR, and this region was thus screened for insertion sites of circularly permuted EGFP (cpEGFP) to yield the most responsive fluorescent sensor. N- and C-terminal amino acids of the insertion linker were individually mutated to optimize the brightness of the sensor. NE1m was developed for multiple uses including *in-vivo* experiments in mice, however, the authors only tested and characterized the sensor for *in-vivo* murine application using fiber photometry. Therefore, towards our goal of understanding NA dynamics during motor learning, I set out to characterize NE1m activity under a two-photon microscope in WT mice throughout the course of learning.

The first objective was to develop a protocol allowing us to consistently image the soma of individual M1 L2/3 pyramidal neurons selectively expressing NE1m. Unfortunately, I found the fluorescence of the NE1m sensor was too dim to adequately identify a consistent somatic signal, and only a limited number of pyramidal somata could be detected in an imaging plane

(Figure 4a). Hence, to visualize the somatic signal, increased laser power was needed. However, in our chronic imaging paradigm, increasing laser power often resulted in bleaching of the fluorophores and cell damage. Notably, despite the low somatic expression of NE1m, I found abundant expression in the neurites (Figure 4b). I thus considered a shift from imaging somatic NE1m activity to imaging the neurites (dendrites and axons).

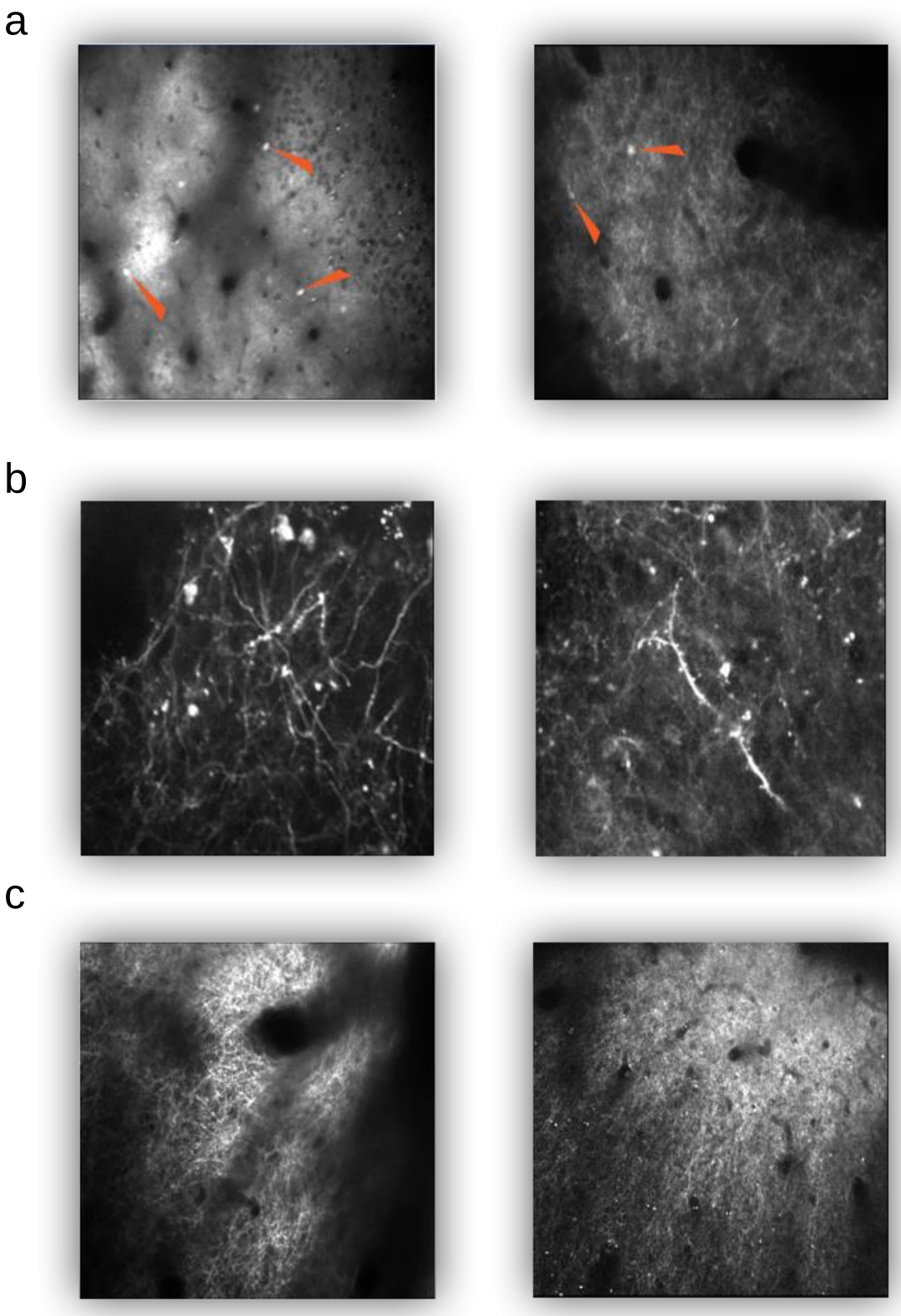

Figure 4: NE1m expression patterns a) somatic expression of NE1m. 600x600µm. Somata are delineated by orange arrows. **b)** dendritic expression of NE1m. 200x200µm. **c)** axonal expression of NE1m. 350x350µm.

In order to visualize the expression of NE1m more clearly in dendritic processes, I systematically tested various dilutions of Cre, in combination with the Cre-dependent NE1m virus, to investigate the possibility of sparsely labelling cells to achieve dendritic expression of NE1m in M1. The intention was to facilitate the selective expression of dendritic fluorescence conducive to spine imaging. While this approach was met with marginal success, this imaging method still required relatively high laser power, and produced similar issues with fluorophore bleaching and cell damaging. I therefore reoriented our approach towards observing NE1m signals in axons (Figure 4c).

Lastly, in order to capture NA activity in M1 throughout the entire course of motor learning while protecting against fluorophore bleaching and cell damage, I restructured our imaging paradigm and imaged only on days 0, 1, 3, 7, 10, and 12 of behavioral training (Figure 5a). This new paradigm has successfully allowed us to observe changes in NA activity in M1 throughout the progression of motor learning without inducing photo-damage in the cells. With these revised methods, I was able to collect reliable chronic imaging data by imaging the axonal gossamer traced by NE1m expression patterns.

Image Segmentation

NE1m Activity Can Be Detected in M1 Neurites

To extract NE1m fluorescence signals from a complex web of axons, there were several important decisions to make in regards to analyzing the fluorescent NA signal. These signal processing decisions are non-trivial, and the novelty of this sensor in both function and design serve only to compound this complexity. Indeed, many software packages have been developed with a specific purpose of developing more standardized imaging analysis pipelines. These types

of programs are attractive for any chronic imaging set up, and in this case especially, due to the long experimental recording time, which would otherwise increase the requirement for manual segmentation and visual inspection of the data. Thus, at the advice of various colleagues, I set out to try a recently developed and popular software: Suite2p[33]. This program is a widely used two-photon imaging pipeline that offers motion correction, automatic segmentation, refinement, signal extraction, and more. Unfortunately, the detection of NE1m expressing neurites by Suite2p was not consistent enough for our use. Therefore, I next considered another software program, CaImAn[34], which includes a signal extraction setting specific to the imaging of neurites. In our hands, however, the results for detecting NE1m activity in neurites were still inconsistent with visual inspection. Several factors may have contributed to the issues faced with Suite2P and CaImAn, including but not limited to: differences in mechanisms between NE1m and more commonly used fluorescent indicators of neural activity (such as GCaMP), differences in membrane expression of NE1m (as compared to other indicators), or differences in rise and decay constants. For both softwares, each of these parameters is required to be set and optimized for extracting fluorescent signals from the sensor being used. Hence, I sought to employ a method that would allow rapid acquisition while maintaining consistency across mice and expression levels, but that would also not require manual image segmentation of a vast and complex network of neurites.

Finally, inspired by a technique used to image neuromodulatory axons in a 2016 publication, I adapted an approach from Howe & Dombeck, wherein dopaminergic axons in striatum, expressing a calcium indicator, GCaMP6, were imaged during locomotion. Their analytical approach consisted of a non-overlapping region of interest (ROI) grid across the entire field of view (FOV), with each ROI encompassing clusters of axons. Using a custom MATLAB

code, I adapted a similar ROI grid to analyze our fluorescence data with a 7x7 grid of non-overlapping ROIs with an area of ~50x50μm each (Figure 5b). This approach produced a more consistent data set, albeit at the cost of some more granular information.

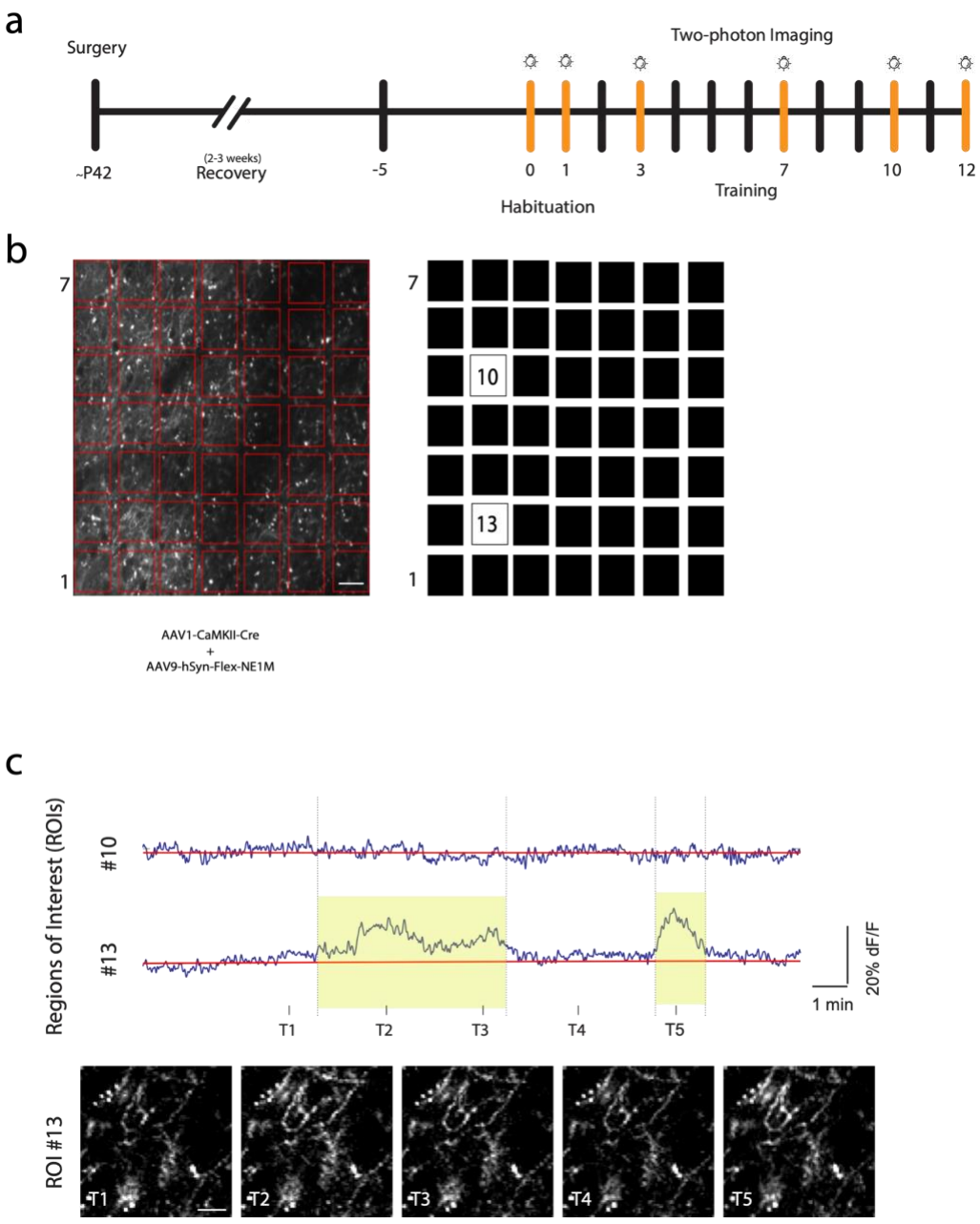

Figure 5: Image segmentation and signal extraction a) two-photon imaging paradigm. Mice undergo craniotomy/injection surgery 42 days postnatal. After 2-3 weeks of recovery, mice are habituated to the spinning-disk under the two-photon microscope for 3-5 days, with 5-10 minutes of habituation each day. On day 0, mice are imaged in the holding tube, without running behavior, to establish a baseline. Mice are subsequently imaged on the 1st, 3rd, 7th, 10th and 12thday of behavior, indicated by the orange coloration and bulbs. **b)** left: overlay of ROI grid on exemplar imaging FOV of mouse injected with NE1m, right: ROI grid alone, highlighting two specific ROIs shown

in **(c)**. scale bar = 100μm. **c)** top: NE1m trace from ROIs indicated in **(b)**, with events highlighted in pale yellow. red solid line, regressed baseline; blue line, smoothed trace; vertical dotted lines/yellow shading, NE1m events; T1-T5, time-points of images below. bottom: five frames of imaging from the time-points indicated above. T2, T3, and T5 are brighter, with the most obvious discrepancies in the top left corner of the ROI. Each ROI is 50x50μm. scale bar = 10μm.

Signal Extraction

NE1m Events Can Be Visually Confirmed

Moving forward, I employed methods similar to Feng et al 2018 to estimate the baseline fluorescence of the NE1m signal using a sliding window to regress over the time series (Figure 5c). This method stood out among other options because it can effectively resolve signal artifacts, providing a reliable estimate even in cases of significant baseline drift. With this baseline estimate, an ROI-specific threshold was calculated (see Methods). Then, I used a custom MATLAB code to detect NA events using estimation criteria (see Methods) based on the duration of experimentally measured NA release found in the literature[36,37]. Notably, these methods yielded results consistent with visual inspection of the two-photon imaging data. With this method of signal extraction established, we can move on to investigate the dynamics of NA release in the motor cortex.

Pharmacology

Selective α2-antagonist Yohimbine Increases NE1m Activity

To confirm that NE1m is responsive to NA activity and responds appropriately to the modulation of NA, I performed additional pharmacological tests to manipulate NA levels via intraperitoneal (IP) injection prior to behavioral testing. Yohimbine is a selective α2-AR-antagonist, and has long been known to increase NA release via suppression of the adrenergic autoreceptors that it targets[38]. In this experiment, I followed our surgery and habituation protocol

(see Methods), and imaged baseline activity (no running) on day 0 for 30 minutes. On the first day of training, an IP injection of saline was administered 30 min prior to the behavioral session. In the following session the next day, I injected yohimbine [0.6mg/ml], (Figure 6a); I observed a robust increase in NE1m activity in multiple regions of M1 (Figure 6b). Critically, the day after the yohimbine session, there was an additional control session with saline, wherein NE1m activity levels did not differ from the saline levels in the first day. These results indicate that NE1m signal is responsive to NA modulation, and faithfully reports NA release in our two-photon imaging paradigm. Together, I have established an experimental pipeline to adequately capture NE1m activity and extract fluorescence signals using *in vivo* two-photon imaging in awake and behaving mice. By analyzing the NE1m activity in M1 neurites, we can now infer the size of NA events in space and time, along with their role in motor learning.

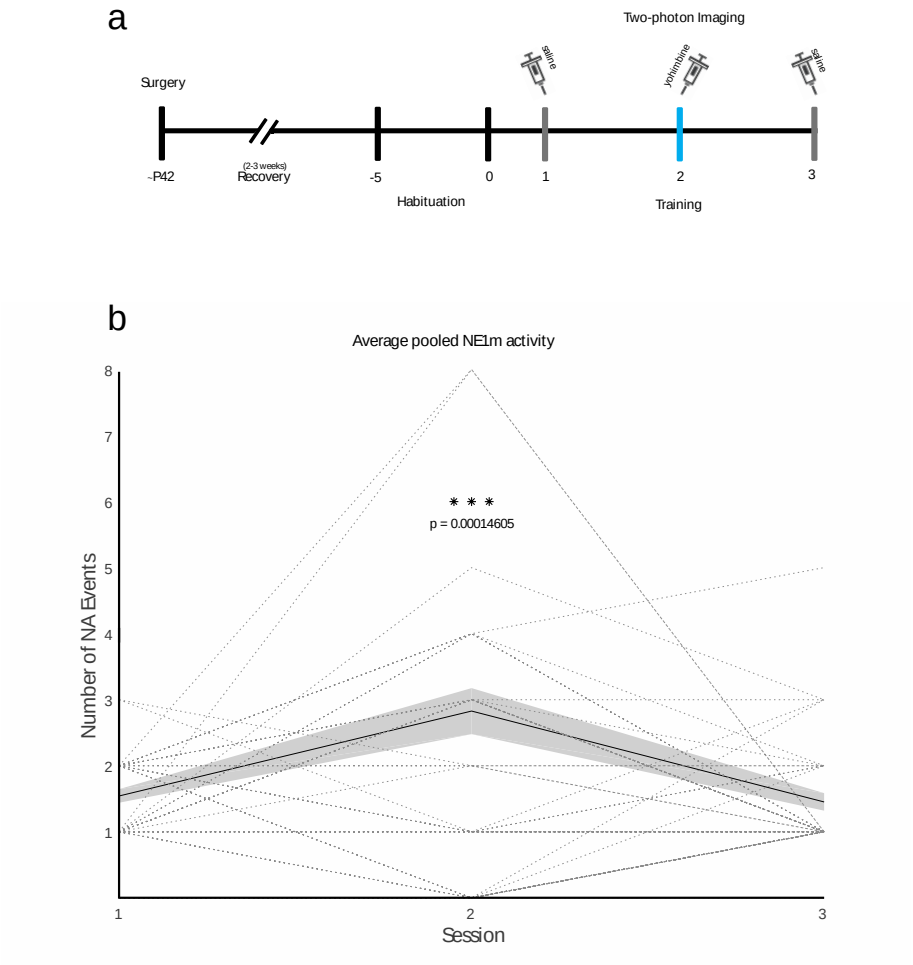

Figure 6: Pharmacological manipulations a) two-photon imaging paradigm with pharmalogical manipulations. Mice undergo craniotomy/injection surgery 42 days postnatal. After 2-3 weeks of recovery, mice are habituated to the spinning-disk under the two-photon microscope for 3-5 days, with 5-10 minutes of habituation each day. On day 0, mice are imaged in the holding tube, without running behavior, to establish a baseline. Mice are subsequently imaged on the first, second, and third days of training. Prior to training, mice underwent IP injection. Days 1 and 3 were saline (grey), on day 2, mice were injected with yohimbine (turquoise). **b)** Average number of NA events increases with yohimbine administration. (***$p < 0.001$; 1-way ANOVA; Solid line, overall average event number from all ROIs, pooled across 2 mice; dashed lines, individual ROIs from 2 mice; shading, s.e.m.).

NA Dynamics During Motor Learning

NA Activity Increases in Early Motor Learning, Followed by a Reduction in Following Sessions

Next, I sought to uncover changes in NE1m dynamics in M1 throughout the course of motor learning. To investigate this question, I imaged the activity levels of NE1m in sessions 0, 1, 3, 7, 10, and 12 of behavioral training. I observed an increase in NE1m activity during the early phase (s1-s3) of learning (Figure 7). Intriguingly, this change took place only after training had begun, as there was no observable difference when I compared the baseline activity of NE1m (session 0) to the activity of the first day of training (Figure 7a). Following an increase in session 3, NA levels return to baseline levels in the late stages of the training, suggesting an important role for NA in the early phase of motor learning (Figure 7b). The high NA levels in early sessions coincide with behavioral exploration and eventually acquiesce to baseline levels in intermediate and late stages of learning as motor strategies are consolidated, delineating the prominent role of NA during the motor learning process. Importantly, each NA release event duration remains consistent throughout motor learning (Figure 7c,d).

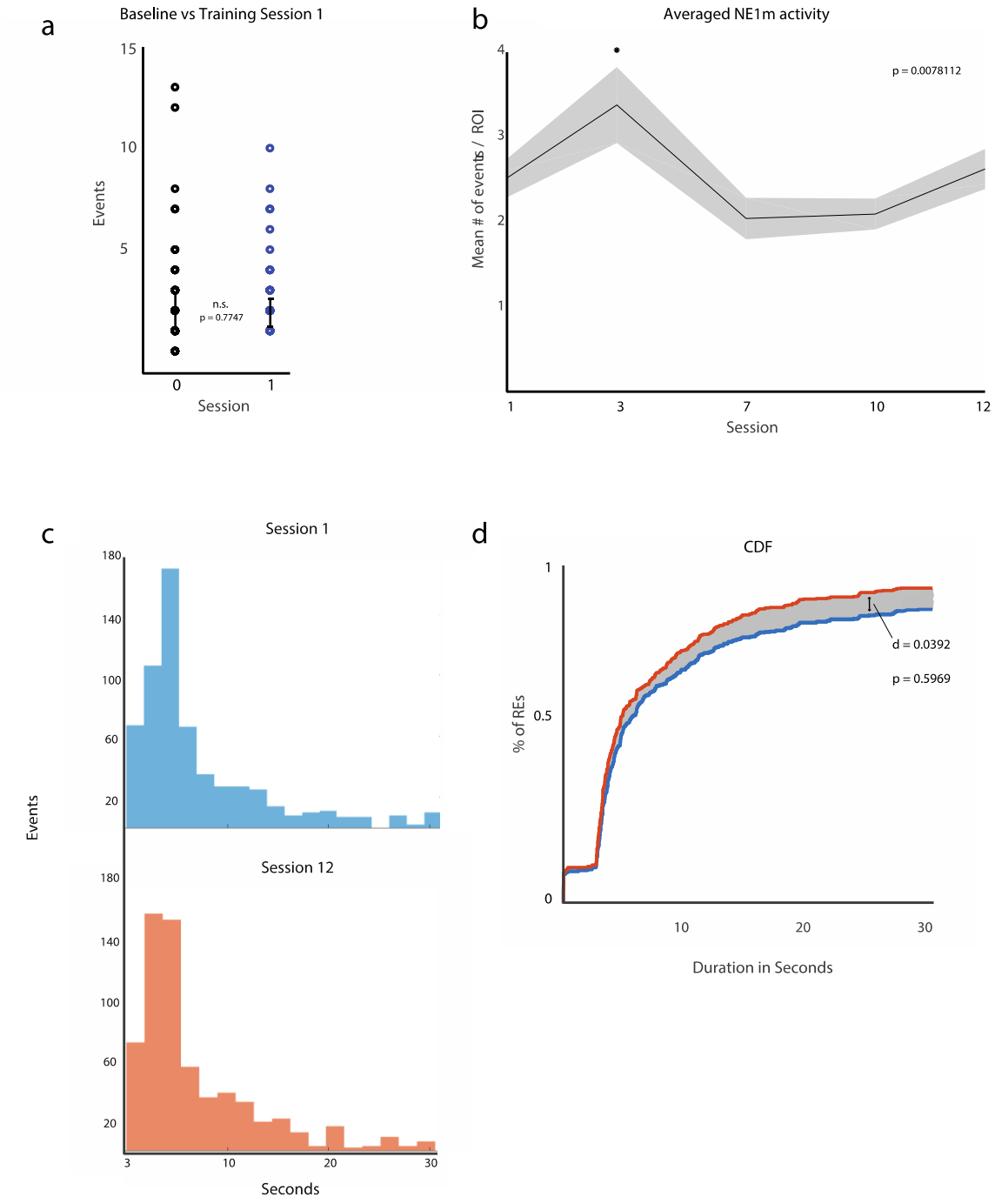

Figure 7: NA activity dynamics in learning a) average number of events does not change between baseline session and the first training session. ($p > 0.8$; Student's t-test; black empty circles, ROIs baseline number of events; black filled circle, average number of baseline events; blue empty circles, ROIs first session number of events; blue filled circle, average number of events in first training session; n=5;bars represent s.e.m.) **b)** mean number of events across all training sessions. We see an early but not immediate increase in NA events per ROI ($p < 0.01$;1-way ANOVA; solid line, average event number per ROI across mice; shading, s.e.m.). **c)** top: histogram of session 1 event duration, bottom: histogram of final session event duration. **d)** cumulative distribution functions (CDF) for first and last sessions indicating no difference between the sessions ($p = 0.5969$; max. distance between distributions, d = 0.039; Kolmogrov-Smirnov test; blue solid line, first session cumulative distribution function; orange solid line, last session cumulative distribution function; grey shaded area, difference between first and last session CDF).

Spatial Auto-correlation

Spatial Clustering of NA Activity Increases in Intermediate Stages of Motor Learning

Motor learning is accompanied by the refinement of spatiotemporal activation patterns of pyramidal cells in M1. Given the influence of NA on motor learning, and its stage-dependent changes in temporal activation in M1, I next set out to investigate the spatial distribution of NA activity to uncover any spatial clustering of NE1m activity across sessions during the motor learning process. Individual heatmaps of event density for sessions 1, 7, and 12 were generated (Figure 8a), and a 2-dimensional autocorrelation matrix for each heatmap was computed (Figure 8b) (see Methods). From this, I observed a substantial relative increase during session 7, compared to session 1 and 12, which may indicate a transient increase in spatial clustering of NA release during intermediate sessions (Figure 8c). Further, first and last sessions have similar rates of autocorrelation, but still show a moderate effect size between them. The intermediate and final sessions exhibit a moderately smaller discrepancy between them, as compared to the discrepancy between the intermediate and first sessions. The slight asymmetry in the comparison between 1:7 and 7:12 may indicate an asymmetrical distribution of NA activity clustering across the motor learning process, where changes in the degree of clustering occur more in one half of the training than the other.

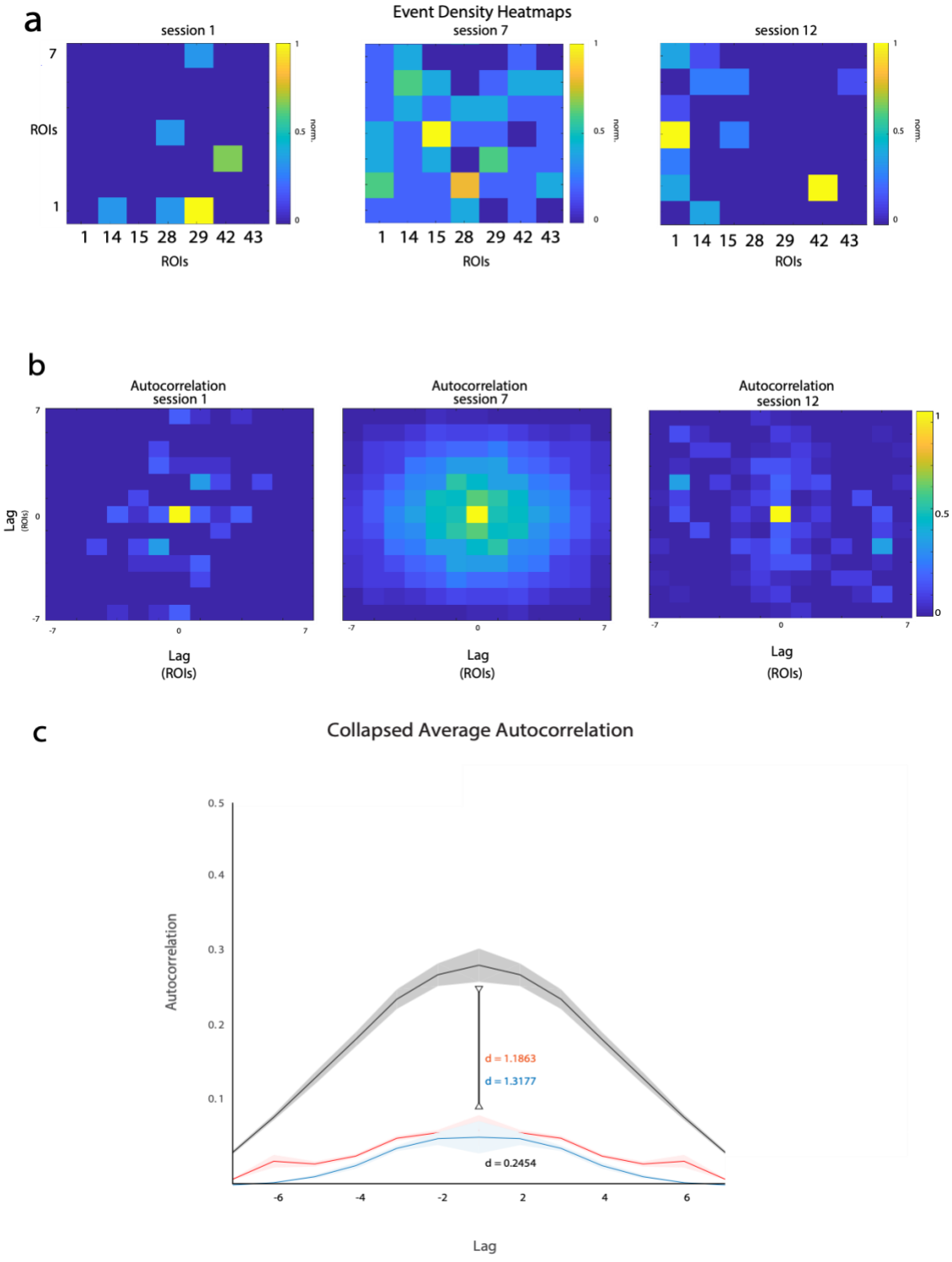

Figure 8: NA spatial activity patterns a) heatmaps of NA event density across imaging FOV for one mouse, left: first session, middle: session 7, right: last session. **b)** autocorrelation heatmaps of the sessions in **(a)**. **c)** degree of autocorrelation, averaged from **(b)** and collapsed along one dimension. Indicates a higher degree of autocorrelation in intermediate sessions (d >1; Cohen's d; blue solid line, average autocorrelation session 1; black solid line, average autocorrelation session 7; orange solid line, average autocorrelation final session; shaded areas represent s.e.m.)

To summarize, early NA increases are released in a somewhat inconsistent spatial pattern. Following an expansion in the distribution of NA events during more spatially clustered intermediate stages, the release pattern is subsequently refined to an alternate—potentially more stable—pattern that is distinct from the distribution of NA in early learning stages. Serendipitously, this expansion and refinement trajectory is complementary to the activity of pyramidal neurons during the motor learning process[19,20], where early learning sees an exploratory attitude from neurons, and consolidation of a motor skill coincides with the fine tuning of relevant neuronal ensembles.

Discussion

The role of neuromodulators in neural activity and in behavior has a rich literature. For example, the role of dopamine (DA) in reward is well established, elevations of acetylcholine (ACh) accompany locomotion and focused attention[23], and NA elevation is typically associated with arousal[39], sensory perception[27], and behavioral flexibility[40,41]. In particular, NA has been receiving increased attention as an effective modulator of behavioral state in favor of optimal outcomes[42]. The results reported here indicate that the increase in NA levels coincides with high variability of behavior during head-fixed motor learning, whereas NA levels returned to baseline levels in expert stages of learning with reduced behavioral variety. Intriguingly, the trajectory of NA activity follows closely the trajectory of pyramidal cortex ensemble activity in WT mice, where highly variable activity patterns emerge in a novel task, and are refined into a distinct pattern of activity with learning.

In regards to the modulation of excitatory and inhibitory activity, NA promotes a dynamic equilibrium, which is a delicate feature of the neocortex often considered dysregulated in ASDs[14]. The adaptive gain theory of LC-NA function, first posited by Cohen and Aston-Jones in 2005, frames LC activity as a modulator of signal amplification via increases in signal-to-noise ratio, which facilitate and promote optimal behavioral performance. Gain increases in this framework then result in increased activity in excited units and decreased activity in inhibited units—a paradigm that lends itself to the role of gating. In order to gate neural activity in motor learning, NA activity may facilitate the potentiation and depression of the appropriate synapses over the course of expansion and refinement.

This thesis reports changes in NA activity during the motor learning process. More precisely, increases in NA activity are seen at an earlier stage of learning. Recent work in our lab

has uncovered a subset of neurons that is activated by running on a head-fixed spinning-disk. This subset of running-related neurons emerges early in the learning process, in sessions 1-3, overlapping with the observed increase in NA levels. Furthermore, in 16p11.2 deletion mice, the running-related subset of neurons exhibited high levels of synchrony in early sessions. 16p11.2 deletion mice exhibit a delay in the acquisition of motor tasks, reduced LC activity, and display a reduction of M1 innervation by LC. These factors all coincide with increased synchrony in early sessions, allowing us to infer that NA is involved with maintaining learning-related cortical activity, potentially acting as a critical gate for excitatory activity.

Indeed, recent publications have identified indicators of adrenergic gating in the hippocampus, acting through K_V channels on dendrites[24], and in the cortex through heterogeneous mechanisms[43]. Our position is thus in line with the notion that NA works to gate M1 activity with critical NA elevations in early stages of learning that wane in the later stages of learning a motor task, following the trajectory of behavioral variability. This role for NA may indicate that local elevations in NA serve to maintain the optimal activation of L2/3 pyramidal neurons during behavioral arousal and locomotion, thereby enabling sparse coding mechanisms to form and consolidate novel ensembles during motor learning.

The consolidation of neuronal ensembles is an important part of the learning process, and may provide a template for neuronal activity. In motor learning for example, learned voluntary movements induce more reproducible neural activity patterns than unfamiliar or untrained voluntary movements. Similarly, variability in motor execution is reduced with learning. In this thesis, I present findings that extend the notion of this learning trajectory to NA activity in the motor learning process (Figure 9). I found that the autocorrelation during the intermediate stages of learning exhibits substantially higher rates compared to session 1 and 12. 2-dimensional

autocorrelation can be thought of as a measure of spatial clustering, indicating an increase in the degree of spatial clustering in intermediate sessions.

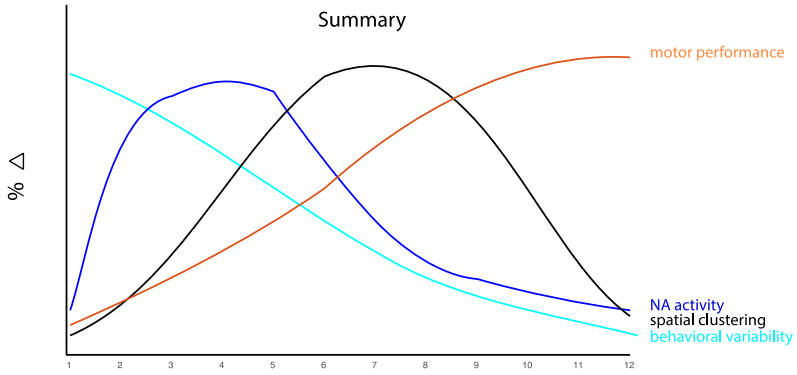

Figure 9: Summary This summary figure highlights the various trajectories of the factors discussed in this thesis. In orange, we see a steady increase in task performance, which approaches a plateau in later sessions. In blue, the change in NA activity across the learning process, with a robust increase in early sessions. The solid black line represents the degree of spatial clustering (as approximated via autocorrelation), which increases in intermediate sessions, and falls back to lower levels in later sessions. Finally, the turquoise line indicates the degree of variability in the behavior according to metrics based on DeepLabCut analysis. Although these curves are a representation only, note the similarity in slope between NA and behavioral variability in later sessions. Similarly, there is a significant degree of overlap between NA activity and the degree of spatial clustering. Finally, note the opposite slope in motor performance compared to NA activity and spatial clustering, and the timing of the performance plateau in comparison to the peak in spatial clustering of NA events.

Understanding the motor learning process can uncover important insights into typical development, as well as awareness of the consequences arising from the disruption thereof. Because these disruptions are so common in ASDs, this awareness will be integral to the development of improved ASD diagnostics that rely on motor skill evaluation and reporting, as well as in treatments related to the early-presenting motor symptoms garnering recent attention in ASD and related fields of study. The results reported in this thesis offer a refreshed view regarding LC-NA involvement in motor skills, with a novel nod at motor skill acquisition. With

consideration of a putative role for NA in motor learning, we can move forward to parse out the details of NA function in the motor cortex. The experimental approach outlined in this thesis in concert with the 16p11.2 deletion mouse model would be a powerful investigative tool for elucidating their motor learning delay, which is rescued by LC-NA activity. Excitingly, the experiments performed also verified the expression and function of NE1m in the cortex, and further optimized this experimental technique for chronic two-photon imaging. Future studies investigating the relationship between NA and motor cortex function during learning in 16p11.2 deletion mice will be important in furthering our understanding of motor learning and the circuit dysfunctions thereof introduced by ASDs.

Methods

Animals

All animal experiments were approved by the University of Ottawa Animal Care Committee in accordance with the Canadian Council on Animal Care guidelines. Mice were group housed in plastic cages with food and water *ad libitum* in a room with a reversed light cycle (12h - 12h). Only male mice aged between 8-14 weeks were used for experiments, and controls were littermates with the same genetic background.

Surgery

Mice were anesthetized under 1-2% isoflurane, and subcutaneous injections of Baytril (10 mg/kg) and buprenorphine (0.1 mg/kg) were performed to reduce infection and analgesia, respectively. An incision was performed to remove a circular piece of the scalp; a custom head-plate was implanted on the skull with instant glue (Krazy Glue) and dental cement (Lang Dental). A craniotomy of approximately 2 mm in diameter was performed over the right motor cortex. Viruses (UPenn Vector Core; calcium imaging: AAV9.CamKII0.4Cre.SV40(1:1, 1:5, 1:500, or 1:1000) and AAV-hSyn-DIO-NE2.1(1:1) diluted in saline, 5 sites, ~35 nL at each site) were injected in the motor cortex around the coordinates (AP: 0.30 mm; ML: 1.5 mm) from bregma, according to previous microstimulation experiments[20,21, 44,45]. Each injection was given at a depth of ~250 μm from the pia, and each injection site was separated by 250 - 500 μm. Each injection was slowly injected over 2 minutes, and the injecting pipette was maintained in the brain for at least 3 minutes in order to prevent backflow. After the virus injections, a custom-made imaging window was implanted over the motor cortex and stabilized with dental acrylic.

Following surgery, mice were given buprenorphine (0.1 mg/kg), and dexamethasone (2 mg/kg). Mice were allowed to recover for 2-3 weeks prior to behavioral testing.

Running Behaviour

Our running disc behavioral task is composed of a 14-cm disk mounted to an axle containing 1024 optical encoders to detect rotational displacements larger than 0.018 cm. Before the task begins, the mouse is head fixed 3cm from the center of the running disk via the head-bar or head-plate implanted during surgery. The disc is highly sensitive to movement, discouraging immobility. Due to the trajectory of the disc and the orientation of the mouse, the mouse must continuously adjust its posture in order to run successfully without interruption. Successful running is defined as reaching and maintaining a velocity of 5cm/s for 3 or more seconds. Each instance of so-defined running is considered an (RE). Mice are habituated to the spinning-disk environment for 3 days prior to the start of training. Habituation includes fixing the head of the mouse to the spinning-disk stage for five minutes a day while the body of the mouse is held stationary by a plastic holding tube. On imaging Day 0, the mouse is imaged under a setup identical to the habituation for the duration of a training session (30 minutes). The next day, training begins and takes place for 12 consecutive days, consisting of 30 (Figures 4-9) or 60 (Figures 1-3) minute sessions each day. Mice underwent 30 minute training sessions for two-photon imaging of NE1m (a preventative measure against bleaching), all of which was performed by me. Mice underwent 60 minute training sessions for experiments performed by Dr. Yin (Figures 1 & 2), and for all DeepLabCut analyses (Figure 3).

DeepLabCut

Locomotive movement analysis was performed using DeepLabCut, which employs a deep neural network to label and track relevant physical features. I recorded mice that underwent head-fixed spinning-disk training over 12 sessions using a high-speed (~100 fps) HD night vision camera (Webcamera_USB). Next, I hand labeled 240 frames of recorded behavior (which were identified by k-means clustering) and trained the network to report the coordinates of the head, neck, thorax, and sacrum of the mice during behavior. To evaluate network performance, the standard package settings were employed against frames in both early and late stages of the behavioral paradigm. As the network reports a confidence estimate with each output coordinate, I additionally filtered out coordinates that were reported with low confidence (<40 %).

To quantify and assess movement variability during an RE, I wrote custom MATLAB code to analyze the corporeal coordinates. By referencing the running data, all coordinates within each RE were isolated, and the X and Y coordinates of the neck were averaged as a vertex. I then used the maximum and minimum Y coordinates (perpendicular to axis of head-fixation) of the sacrum during running to draw lines connecting the two extreme sacrum points with the vertex, and calculated the vertex angle as an index of displacement (in degrees) for each RE (Figure 3c). Lastly, the relative variance of the angles from all REs in each session was calculated with the formula:

$$Relative\ Variance = \frac{{sd_A}^2}{|\mu_A|}$$

where A is a normalized set of angles generated in the REs of a recorded behavioral session.

Two-Photon Image Acquisition

Imaging was performed with a commercial two-photon microscope (B-scope, Thorlabs) using a 16× objective (NIKON) with excitation at 925 nm (InSight X3, Spectra-Physics) at 30 Hz. For calcium imaging, one plane of images (512 × 512 pixels covering 350 × 350 μm) was acquired at ~250 μm (L2/3) from pia continuously while mice were running on the rotating disk. The same imaging plane was followed in every session. Mice were habituated under head-fixation inside a plastic holding tube for 5 minutes/day for 3 days prior to training and imaging.

Image Analysis

Lateral motion was corrected using full-frame cross-correlation image alignment (Turboreg plug-in ImageJ). A custom MATLAB program[12] was used to manually draw a 7x7 grid, resulting in 49 ROIs. The same ROIs were followed across all sessions. Fluorescence traces for each ROI were generated by averaging pixels within the ROI. After passing the raw fluorescence time-series through non-linear median and linear Gaussian filters, the baseline (F_0) fluorescence was approximated using the MATLAB function 'msbackadj', using a sliding window ~10% of the recording duration to regress over the filtered time series. The formula $(F_{raw} - F_0)/ F_0$ was then used to calculate instantaneous $\Delta F/F$.

Activity Analysis

NA activity was defined by events consisting of an instance of ΔF/F rising above a threshold, calculated on an individual ROI basis, for 90 frames (3 seconds) of imaging. This duration is based on studies investigating the time course of NA release[36,37], and development and expression of the sensor[35]. The event threshold was determined by: $F_0 + (2.5 \times std_{F0})$

Event frequency was analyzed by using the stated criteria to define an event on an individual ROI basis, and then taking the mean number of events for all active ROIs pooled across mice by session. Baseline activity was collected by imaging non-training mice with their movements restrained by a plastic holding tube on the day prior to the initiation of training. Baseline imaging was collected following 3-5 days of habituation of 5-10 minutes in the holding tube under the experimental imaging set-up.

Spatiotemporal activity was analyzed by calculating the autocorrelation of each event density heatmap generated. Comparing the summed event number per ROI in a pair-wise manner resulted in a 2-dimensional autocorrelation matrix. The cross-correlation of matrix X, of size M-by-N, and matrix Y, of size P-by-Q, is matrix Z, of size M+P-1 by N+Q-1. Thus, with 7-by-7 heatmaps, our cross-correlation matrices are of size 13-by-13. The cross-correlation value in row *k* and column *l* of matrix Z is given by: $\sum_{m=0}^{M-1}\sum_{n=0}^{N-1} X(m,n)H\,(m-k,n-l)$. Correlation coefficients were averaged by column to be collapsed into 1-dimension. I then compared these averages using Cohen's d as a measure of effect size.

Pharmacological Manipulations

Mice underwent the surgical procedure outlined above. Following recovery, mice were habituated to the spinning-disk under the two-photon microscope for 3-5 days. On day 1 and 3,

mice received an IP injection of saline 30 mins prior to running. On the second day, mice received an IP injection of 0.6mg/ml (3mg/kg) yohimbine.

Statistical Analyses

For all experiments in this study using 16p11.2 deletion mice, experimenters were blinded to the manipulations and genotypes of animals. All statistical analyses were performed using MATLAB, and all values were reported as mean ± s.e.m. Statistical significance was determined via bootstrap test, 1-way ANOVA with Bonferroni corrections, Student's T-test, or Kolmogrov-Smirnov. Effect size was computed using Cohen's d. Two-tailed tests were used for all comparisons unless indicated.

Disclaimer

Experiments in Figure 1 and 2 were performed by the post-doc Dr. Xuming Yin in a project preceding my thesis. For the experiment in Figure 6, injection and data acquisition were performed by myself and Dr. Yin, and I performed the data analysis. I performed the rest of the surgeries, and data in all other experiments were collected and analyzed by me.

Index

Figures

Legend

LC – locus coeruleus

NA – noradrenaline (norepinephrine)

ASD – Autism Spectrum Disorder

M1 – primary motor cortex

L2/3 – layer 2/3 pyramidal neurons

DREADD – designer receptors exclusively activated by designer drugs

WT – wild type

RE – running epoch

V_r – relative variance

CV – coefficient of variance

AR – adrenergic receptors

ICL_3 – third intracellular loop

cpEGFP – circularly permuted enhanced green fluorescent protein

GCamP – GFP, calmodulin, and M13, a peptide

ROI – region of interest

FOV – field of view

IP – intraperitoneal

CDF – cumulative distribution function

DA – dopamine

ACh – acetylcholine

References

1. Kleinman, Jamie M., et al. “Diagnostic Stability in Very Young Children with Autism Spectrum Disorders.” *Journal of Autism and Developmental Disorders*, vol. 38, no. 4, 2007, pp. 606–615., doi:10.1007/s10803-007-0427-8.
2. Lebarton, Eve Sauer, and Jana M. Iverson. “Associations between Gross Motor and Communicative Development in at-Risk Infants.” *Infant Behavior and Development*, vol. 44, 2016, pp. 59–67., doi:10.1016/j.infbeh.2016.05.003.
3. Libertus, Klaus, et al. “Limited Fine Motor and Grasping Skills in 6-Month-Old Infants at High Risk for Autism.” *Child Development*, 2014, doi:10.1111/cdev.12262.
4. Hampton, L. H., and A. P. Kaiser. “Intervention Effects on Spoken-Language Outcomes for Children with Autism: a Systematic Review and Meta-Analysis.” *Journal of Intellectual Disability Research*, vol. 60, no. 5, 2016, pp. 444–463., doi:10.1111/jir.12283.
5. Dawson, G., et al. “Randomized, Controlled Trial of an Intervention for Toddlers With Autism: The Early Start Denver Model.” *Pediatrics*, vol. 125, no. 1, 2009, doi:10.1542/peds.2009-0958.
6. Gernsbacher, Morton Ann, et al. “Infant and Toddler Oral- and Manual-Motor Skills Predict Later Speech Fluency in Autism.” *Journal of Child Psychology and Psychiatry*, vol. 49, no. 1, 2008, pp. 43–50., doi:10.1111/j.1469-7610.2007.01820.x.
7. Bedford, Rachael, et al. “Early Gross Motor Skills Predict the Subsequent Development of Language in Children with Autism Spectrum Disorder.” *Autism Research*, vol. 9, no. 9, 2015, pp. 993–1001., doi:10.1002/aur.1587.

8. Portmann, Thomas, et al. “Behavioral Abnormalities and Circuit Defects in the Basal Ganglia of a Mouse Model of 16p11.2 Deletion Syndrome.” *Cell Reports*, vol. 7, no. 4, 2014, pp. 1077–1092., doi:10.1016/j.celrep.2014.03.036.
9. Yin et al 2020, *under review*
10. Chen, Tsai-Wen, et al. “A Map of Anticipatory Activity in Mouse Motor Cortex.” *Neuron*, vol. 94, no. 4, 2017, doi:10.1016/j.neuron.2017.05.005.
11. Masamizu, Yoshito, et al. “Two Distinct Layer-Specific Dynamics of Cortical Ensembles during Learning of a Motor Task.” *Nature Neuroscience*, vol. 17, no. 7, 2014, pp. 987–994., doi:10.1038/nn.3739.
12. Cichon, Joseph, and Wen-Biao Gan. “Branch-Specific Dendritic Ca2+ Spikes Cause Persistent Synaptic Plasticity.” *Nature*, vol. 520, no. 7546, 2015, pp. 180–185., doi:10.1038/nature14251.
13. Heindorf, Matthias, et al. “Mouse Motor Cortex Coordinates the Behavioral Response to Unpredicted Sensory Feedback.” *Neuron*, vol. 101, no. 6, 2019, p. 1202., doi:10.1016/j.neuron.2019.02.042.
14. London, Eric B. “Neuromodulation and a Reconceptualization of Autism Spectrum Disorders: Using the Locus Coeruleus Functioning as an Exemplar.” *Frontiers in Neurology*, vol. 9, 2018, doi:10.3389/fneur.2018.01120.
15. Nelson, Sacha B., and Vera Valakh. “Excitatory/Inhibitory Balance and Circuit Homeostasis in Autism Spectrum Disorders.” *Neuron*, vol. 87, no. 4, 2015, pp. 684–698., doi:10.1016/j.neuron.2015.07.033.
16. Inoue, Masato, et al. “Error Signals in Motor Cortices Drive Adaptation in Reaching.” *Neuron*, vol. 90, no. 5, 2016, pp. 1114–1126., doi:10.1016/j.neuron.2016.04.029.

17. Pruszynski, J. Andrew, et al. “Primary Motor Cortex Underlies Multi-Joint Integration for Fast Feedback Control.” *Nature*, vol. 478, no. 7369, 2011, pp. 387–390., doi:10.1038/nature10436.
18. Karni, A., et al. “The Acquisition of Skilled Motor Performance: Fast and Slow Experience-Driven Changes in Primary Motor Cortex.” *Proceedings of the National Academy of Sciences*, vol. 95, no. 3, 1998, pp. 861–868., doi:10.1073/pnas.95.3.861.
19. Wu, Howard G, et al. “Temporal Structure of Motor Variability Is Dynamically Regulated and Predicts Motor Learning Ability.” *Nature Neuroscience*, vol. 17, no. 2, 2014, pp. 312–321., doi:10.1038/nn.3616.
20. Peters, A. J., Chen, S. X. & Komiyama, T. Emergence of reproducible spatiotemporal activity during motor learning. *Nature* **510**, 263-267, doi:nature13235 [pii]
21. Chen, S. X., Kim, A. N., Peters, A. J. & Komiyama, T. Subtype-specific plasticity of inhibitory circuits in motor cortex during motor learning. *Nature neuroscience* **18**, 1109-1115, doi:10.1038/nn.4049 (2015).
22. Makino, Hiroshi, et al. “Transformation of Cortex-Wide Emergent Properties during Motor Learning.” *Neuron*, vol. 94, no. 4, 2017, doi:10.1016/j.neuron.2017.04.015.
23. Garcia-Junco-Clemente, Pablo, et al. “State-Dependent Subnetworks of Parvalbumin-Expressing Interneurons in Neocortex.” *Cell Reports*, vol. 26, no. 9, 2019, doi:10.1016/j.celrep.2019.02.005.
24. Liu, Yanling, et al. “Adrenergic Gate Release for Spike Timing-Dependent Synaptic Potentiation.” *Neuron*, vol. 93, no. 2, 2017, pp. 394–408., doi:10.1016/j.neuron.2016.12.039.

25. Labarrera, Christina, et al. “Adrenergic Modulation Regulates the Dendritic Excitability of Layer 5 Pyramidal Neurons In Vivo.” *Cell Reports*, vol. 23, no. 4, 2018, pp. 1034–1044., doi:10.1016/j.celrep.2018.03.103.

26. Schiemann, Julia, et al. “Cellular Mechanisms Underlying Behavioral State-Dependent Bidirectional Modulation of Motor Cortex Output.” *Cell Reports*, vol. 11, no. 8, 2015, pp. 1319–1330., doi:10.1016/j.celrep.2015.04.042.

27. Martins, Ana Raquel O, and Robert C Froemke. “Coordinated Forms of Noradrenergic Plasticity in the Locus Coeruleus and Primary Auditory Cortex.” *Nature Neuroscience*, vol. 18, no. 10, 2015, pp. 1483–1492., doi:10.1038/nn.4090.

28. Uematsu, Akira, et al. “Modular Organization of the Brainstem Noradrenaline System Coordinates Opposing Learning States.” *Nature Neuroscience*, vol. 20, no. 11, 2017, pp. 1602–1611., doi:10.1038/nn.4642.

29. Chandler, D. J., et al. “Heterogeneous Organization of the Locus Coeruleus Projections to Prefrontal and Motor Cortices.” *Proceedings of the National Academy of Sciences*, vol. 111, no. 18, 2014, pp. 6816–6821., doi:10.1073/pnas.1320827111.

30. Schwarz, Lindsay A., et al. “Viral-Genetic Tracing of the Input–Output Organization of a Central Noradrenaline Circuit.” *Nature*, vol. 524, no. 7563, 2015, pp. 88–92., doi:10.1038/nature14600.

31. Gonçalves, J Tiago, et al. “Circuit Level Defects in the Developing Neocortex of Fragile X Mice.” *Nature Neuroscience*, vol. 16, no. 7, 2013, pp. 903–909., doi:10.1038/nn.3415.

32. Peça, João, et al. “Shank3 Mutant Mice Display Autistic-like Behaviours and Striatal Dysfunction.” *Nature*, vol. 472, no. 7344, 2011, pp. 437–442., doi:10.1038/nature09965.

33. Pachitariu, Marius, et al. “Suite2p: Beyond 10,000 Neurons with Standard Two-Photon Microscopy.” 2016, doi:10.1101/061507.

34. Giovannucci, Andrea, et al. “CalmAn: An Open Source Tool for Scalable Calcium Imaging Data Analysis.” 2018, doi:10.1101/339564.

35. Feng, Jiesi, et al. “A Genetically Encoded Fluorescent Sensor for Rapid and Specific in Vivo Detection of Norepinephrine.” 2018, doi:10.1101/449546.

36. Teschemacher, A.g. “Real-Time Measurements of Noradrenaline Release in Periphery and Central Nervous System.” *Autonomic Neuroscience*, vol. 117, no. 1, 2005, pp. 1–8., doi:10.1016/j.autneu.2004.10.002.

37. Courtney, N. A., and C. P. Ford. “The Timing of Dopamine- and Noradrenaline-Mediated Transmission Reflects Underlying Differences in the Extent of Spillover and Pooling.” *Journal of Neuroscience*, vol. 34, no. 22, 2014, pp. 7645–7656., doi:10.1523/jneurosci.0166-14.2014.

38. Johnson, Richard William, et al. “Effects of Desipramine and Yohimbine on α2- and β-Adrenoreceptor Sensitivity.” *European Journal of Pharmacology*, vol. 67, no. 1, 1980, pp. 123–127., doi:10.1016/0014-2999(80)90019-9.

39. Breton-Provencher, Vincent, and Mriganka Sur. “Active Control of Arousal by a Locus Coeruleus GABAergic Circuit.” 2018, doi:10.1101/412338.

40. Bouret, Sebastien, and Susan J. Sara. “Network Reset: a Simplified Overarching Theory of Locus Coeruleus Noradrenaline Function.” *Trends in Neurosciences*, vol. 28, no. 11, 2005, pp. 574–582., doi:10.1016/j.tins.2005.09.002.

41. Glennon, Erin, et al. “Locus Coeruleus Activation Accelerates Perceptual Learning.” *Brain Research*, vol. 1709, 2019, pp. 39–49., doi:10.1016/j.brainres.2018.05.048.

42. Aston-Jones, G., and B. Waterhouse. “Locus Coeruleus: From Global Projection System to Adaptive Regulation of Behavior.” *Brain Research*, vol. 1645, 2016, pp. 75–78., doi:10.1016/j.brainres.2016.03.001.

43. Huang, S., et al. “Adrenergic Gating of Hebbian Spike-Timing-Dependent Plasticity in Cortical Interneurons.” *Journal of Neuroscience*, vol. 33, no. 32, 2013, pp. 13171–13178., doi:10.1523/jneurosci.5741-12.2013.

44. Xu, T. *et al.* Rapid formation and selective stabilization of synapses for enduring motor memories. *Nature* **462**, 915-919, doi:nature08389 [pii]

45. Ayling, O. G., Harrison, T. C., Boyd, J. D., Goroshkov, A. & Murphy, T. H. Automated light-based mapping of motor cortex by photoactivation of channelrhodopsin-2 transgenic mice. *Nature methods* **6**, 219-224, doi:10.1038/nmeth.1303 (2009).